IEEE Access
Multidisciplinary | Rapid Review | Open Access Journal

Received November 21, 2018, accepted December 7, 2018, date of publication December 13, 2018,
date of current version January 7, 2019.

Digital Object Identifier 10.1109/ACCESS.2018.2886641

A Meta-Surface Decoupling Method for Two Linear Polarized Antenna Array in Sub-6 GHz Base Station Applications

FENG LIU, (Student Member, IEEE), JIAYIN GUO, LUYU ZHAO, (Member, IEEE), XIUMEI SHEN, AND YINGZENG YIN

Key Laboratory of Antennas and Microwave Technologies, Xidian University, Xi'an 710071, China

Corresponding author: Luyu Zhao (lyzhao@xidian.edu.cn)

This work was supported by the Natural Science Foundation of China under Grant 61701366 and Grant 61501340.

ABSTRACT In this paper, an extremely compact two-element linear polarized multiple-input-multiple-output (MIMO) antenna array with a metasurface superstrate is proposed. Instead of using periodic square split-ring resonators which occupy larger space and which are incident angle variant, double-layer short wire is utilized as the unit cell of the metasurface. The metasurface is compact in size and effective in decoupling two nearby Bowtie antennas strongly coupled in the H-plane with the spacing of only 0.27 wavelength. After decoupling, the isolation between the two antennas has been improved from around 10 dB to more than 25 dB within the band of 2300 to 2690 MHz while their reflection remained below −15 dB. Moreover, the radiation pattern after adding the metasurface superstrate is well maintained with total efficiency improvement by about 10%, and the envelope correlation coefficient between the two antennas is reduced from 0.35 to below 0.12 within the whole band of interest. The proposed method can find plenty of applications in MIMO and 5G communication systems.

INDEX TERMS Antenna array mutual coupling, base station, decoupling, multiple-input-multiple-output (MIMO), metamaterial, meta-surface, 5G.

I. INTRODUCTION

As the advance of fifth generation (5G) wireless communication systems, there has been a revolution in antenna techniques [1], [2]. The introduction of multiple-input-multiple-output (MIMO) technique, although promising transmission rate avalanche, makes it more difficult to implement antenna under stringent size constraint. The antenna decoupling problem, aiming at reducing antenna mutual coupling, has received great attention in the past ten years.

The many existing and emerging mutual coupling reduction/decoupling methods [3], although are various in theory and implementation, can be classified into the following five categories:

(1) The network based decoupling solution [4]–[15]: Passive or active microwave networks are designed and connected to the antennas to reduce their mutual coupling. Based on the manner of connection, they can be further divided into three types:

(a) *Parallel connected decoupling networks*: The network is in shunt with the coupled antennas, admittance parameters are therefore utilized to design and synthesis those networks. The decoupling network can be a section of transmission line whose characteristic impedance is designed to cancel out antenna mutual coupling [4]; a lumped element with extra matching networks [5]; coupled resonator decoupling networks that can be directly synthesized. The CRDN can be used for two MIMO antennas operating in single band [6] and dual-band [7]. Furthermore, they can also be applied to reduce the interference for antennas resonating in adjacent frequency bands [8].

(b) *Decoupling Networks that are cascaded with antennas*: Mode decomposition networks that are composed of couplers, which can diagonalize the scattering matrix of coupled antennas, have been proposed for many years. Theoretically it can be applied to all kinds of arrays and antennas [9], [10], however, since the excited modes are quite different in Q and radiation pattern, this method is not suitable for MIMO systems. Complex transmission line networks as cascaded decoupling networks have also been invented [11]. The CRDN also has a cascaded version, which is demonstrated in [12].

(c) *The neutralization line decoupling method*: Lines with certain lengths and widths connecting to the coupled antennas are also proposed in many papers. The method is proved to be effective for mobile phone antennas that are relatively narrow band [13], for wideband antennas [14] and even for UWB antennas [15]. The lines not only introduce an inverse path for mutual coupling cancellation, they also perturb the radiated near field of the coupled antennas.

(2) The parasitic element(s) decoupling solution [16]–[19]: Parasitic decoupling, such as monopoles [16], PIFAs [17], mushroom-like structures [18] and parasitic elements as superstrate [19], can also achieve the purpose of decoupling antennas. The parasitic elements in all these cases must be carefully designed such that the original antenna radiation pattern will not be distorted, and the matching performance will not deteriorate.

(3) The ground modification decoupling solution [20]–[25]: Cutting slot on ground plane is a very simple way to decouple antennas, although the slot itself may also resonant. It can be applied to PIFA antennas [20], patch antennas [21] and UWB antennas [22]. The defected ground structures have been proposed for a long time [23] and can take various forms. They can be periodically arranged [23], fractal [24], or symmetrical [25]. The DGS is able to create bandstop characteristic within the band of interest.

(4) The pattern, space or mode-based diversity solution [26]–[29]: Using directive radiation patterns to intentionally create orthogonality in multiple antennas has been proposed in [26]. Meanwhile, the characteristic mode method has been widely used in MIMO antenna designs because of its mode- based diversity [27]–[29]. Since the mode orthogonality can be disturbed by antenna housing, feeding lines and other nearby environment, people have to carefully design these modes considering the abovementioned factors.

(5) The meta-material based or inspired decoupling solution: The number of literatures utilizing the concept of meta-material for antenna decoupling purpose is dramatically increasing these years [30]–[43]. The many existing methods can also be further divided into four types:

a) Electromagnetic Band Gap (EBG) or High Impedance Surface (HIS) based solution: Since [30] used EBG structures between two patch antennas to increase isolation, there are many similar literatures [31]–[36]. To apply this method in antenna decoupling, enough spacing between antenna elements must be ensured to deploy enough EBG cells.
b) Spoof Surface Plasmon Polariton (SSPP) based solution [37], where decoupling between microstrip antennas is achieved utilizing the low-pass nature of SSPP lines.
c) Meta-cloak/wall solution: metamaterial based decoupling walls are proposed in [38]–[40] and metasurface cloaks are used in [41] to reduce mutual coupling by near field transformation.
d) Meta-superstrate based solution: Decoupling antennas using metamaterials demands enough spacing between antennas in most of the cases. To overcome this shortcoming, meta-superstrate decoupling method has been proposed recently [42], [43]. It makes a tradeoff between antenna profile and inter-antenna isolation and could be very effective when inter-antenna spacing is stringent.

This paper proposed a very simple and compact meta-superstrate for two closely packed vertically polarized base-station antenna elements. Compared to many existing decoupling technologies, it has the following unique features:

1) The proposed metasurface is made up of dual layer cut wires which is compact in size, incident angle invariant and most importantly, it will not deteriorate the antenna's original cross polarization discrimination (XPD) compared to the authors' previous work [43], where the SRRs in the metasurface lead to poor XPD.
2) Using the Meta-Surface Antenna Array Decoupling Method (MAAD) and with the metasurface, the inter-element spacing can be reduced to about 0.27 wavelength while maintaining more than 25dB isolation and better than 15dB matching simultaneously.
3) It is proved, for the first time, that these meta-superstrate methods for decoupling purpose can be applied to antennas with more than 15% fractional bandwidth (FBW). While in [42] and [43] the operational FBW are no more than 7%.

The remaining parts of the paper will be organized in the following way: Section II will briefly introduce the metasurface design with cut wires as unit cell and make comparison with its previous SRR version [43], followed by antenna design with the metasurface in Section III. After discussing the measurement results in Section IV, Section V will make conclusions.

II. METASURFACE UNIT CELL DESIGN AND ANALYSIS

According to the design theory illustrated in [43], two antennas in close proximity with the metasurface, together with their respective field components are shown in Fig. 1. The anisotropic nature of the meta-surface superstrate caused by equivalent negative permeability transforms the radiating wave into z-direction and rejects its x-component. Mutual coupling is therefore successfully reduced.

To make the meta-surface compact, double layer cut wire [44] is used as the unit cell which is shown in Fig. 2 (a). The equivalent circuit model is also shown in Fig. 2 (b). The wires themselves contribute mainly to the inductance L while the capacitance C is created between the upper and lower cut wires. Their ideal values can be calculated as:

$$L = \frac{\mu_0 \cdot (ld \cdot Hs)}{t}, \tag{1}$$

and

$$C = \frac{\varepsilon_r \cdot \varepsilon_0 \cdot (ld \cdot t)}{Hs} \tag{2}$$

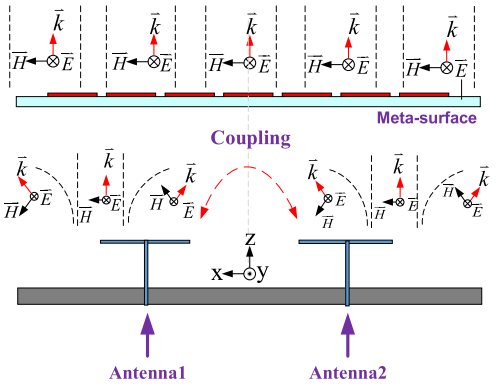

FIGURE 1. Respective field components of the two coupled antennas with the proposed metasurface. Stray coupling is successfully rejected by the metasurface composed of periodic cut wires.

Therefore, the magnetic resonant frequency of the unit cell is written as:

$$f_m = \frac{1}{2\pi\sqrt{L \cdot C}} = \frac{c_0}{2\pi \cdot ld \cdot \sqrt{\varepsilon_r}} \tag{3}$$

where c_0 is the speed of light in vacuum. According to (3), the resonant frequency is inversely proportional to the wire length.

One advantage to use the cut wires as the unit cell of metasurface is its incident angle invariant characteristic, which is illustrated in Fig. 2. In Fig. 2 (c) & (d), the magnitude and phase of the reflection coefficients with respect to different incident wave angles θ are superposed. It is clear that the resonant frequencies are almost unchanged. As a counterpart, we also simulate SRR as the unit cell of metasurface as shown in Fig. 3 (a). The magnitude and phase of the reflection coefficients with respect to different incident wave angles θ are plotted in Fig. 3 (b) & (c). As the angle θ varies, the resonant frequency of the unit cell changes significantly.

To further illustrate the characteristics of the metasurface with cut-wire pairs, the effective permittivity and permeability of the metasurface unit are calculated by using the standard retrieval methods [45] and the results are shown in Fig. 4. From Fig.4 (a), it can be seen that, in 2.5GHz frequency band, the real part of the equivalent permeability is negative while the real part of the equivalent permittivity is positive. Moreover, if we manipulate the length of the cut wires *ld* as shown in Fig. 4 (b), the negative permeability region can be easily controlled.

III. ANTENNA DESIGN USING MAAD METHOD

A. INITIAL ANTENNA DESIGN

To verify the effectiveness of the decoupling method proposed in this paper, the geometry of the initial MIMO antenna as a reference antenna is shown in Fig. 5. A conventional bowtie dipole antenna is used as the initial antenna, and in order to make the antenna relatively wideband, the antenna adopts a T-shape feed structure. Both the antenna and the feed structure are printed on a FR4 substrate having the height

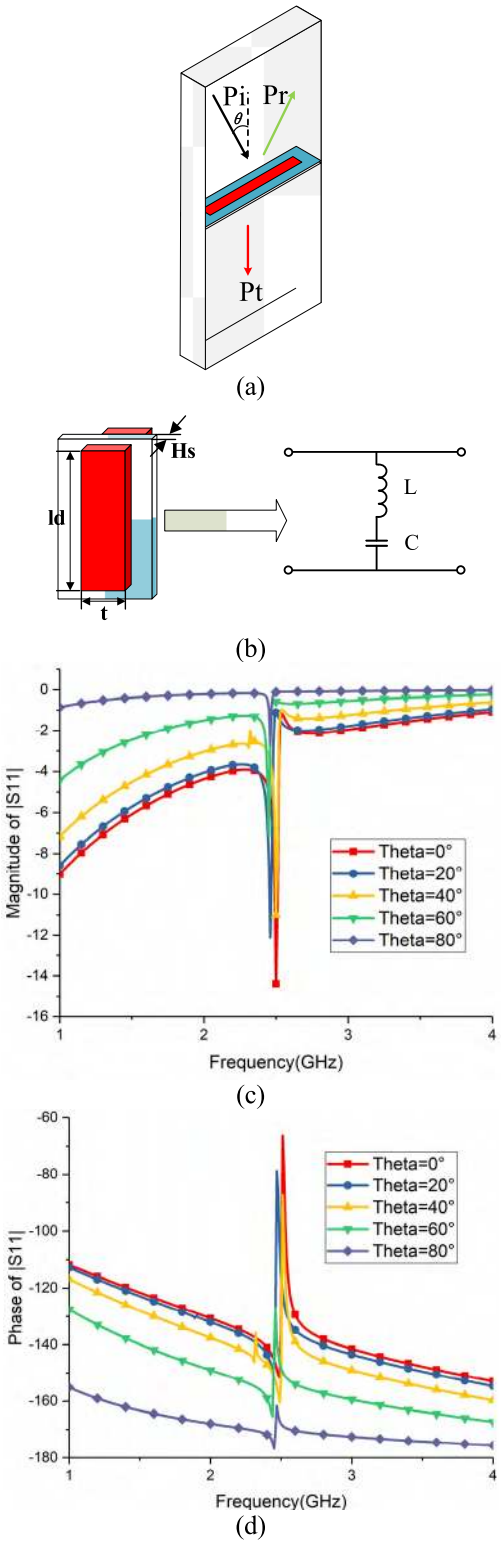

FIGURE 2. (a) The double layer cut wires as the unit cell. (b) The equivalent circuit of the cut wires. (c) The magnitude and; (d)The phase of the reflection coefficients with respect to different incident wave angles θ.

of 1mm and with relative dielectric constant of 4.4 and the loss tangent of 0.02. The design is similar to that in [46] although only vertical polarization is realized. The two

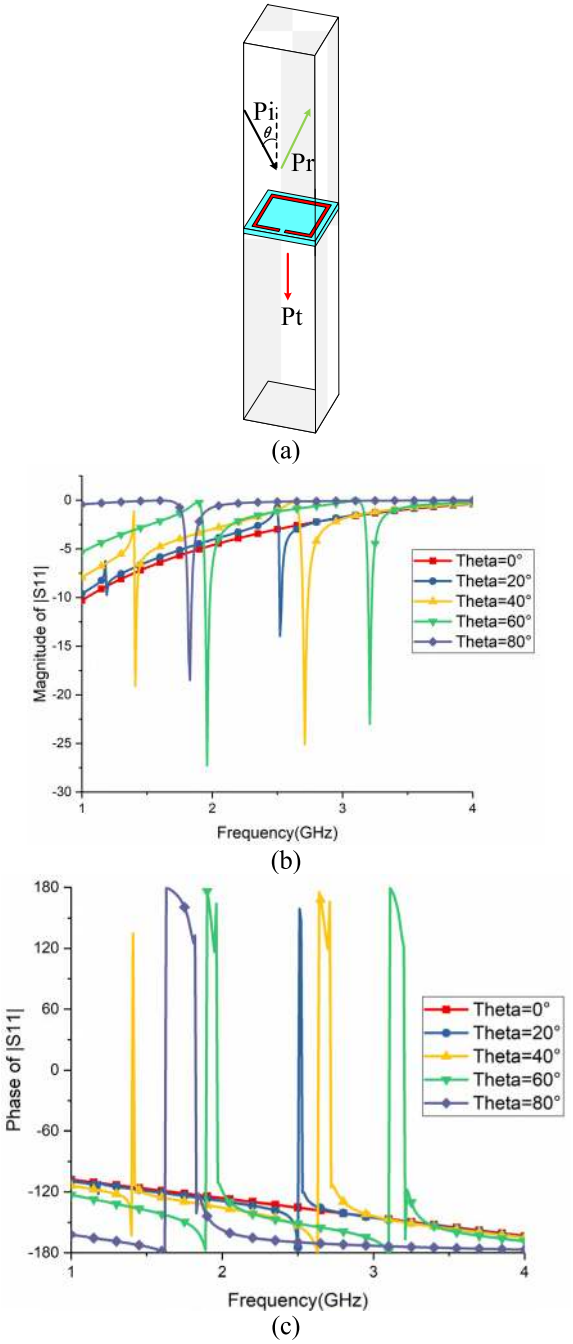

FIGURE 3. (a) The SRR as the unit cell. (b) The magnitude and; (c) The phase of the reflection coefficients with respect to different incident wave angles θ.

antennas are coupled in H-plane with center to center distance: Ly = 33mm (0.27 λ_0 at 2.5GHz). Other specific design parameters are shown in Table 1.

The antennas are fabricated and measured using Keysight E5080 network analyzers. The results are displayed in Fig. 6. It is obvious that although the antennas are well matched from 2300 to 2690 MHz with reflection better than −15dB, the isolation is only about 10dB within the band of interest.

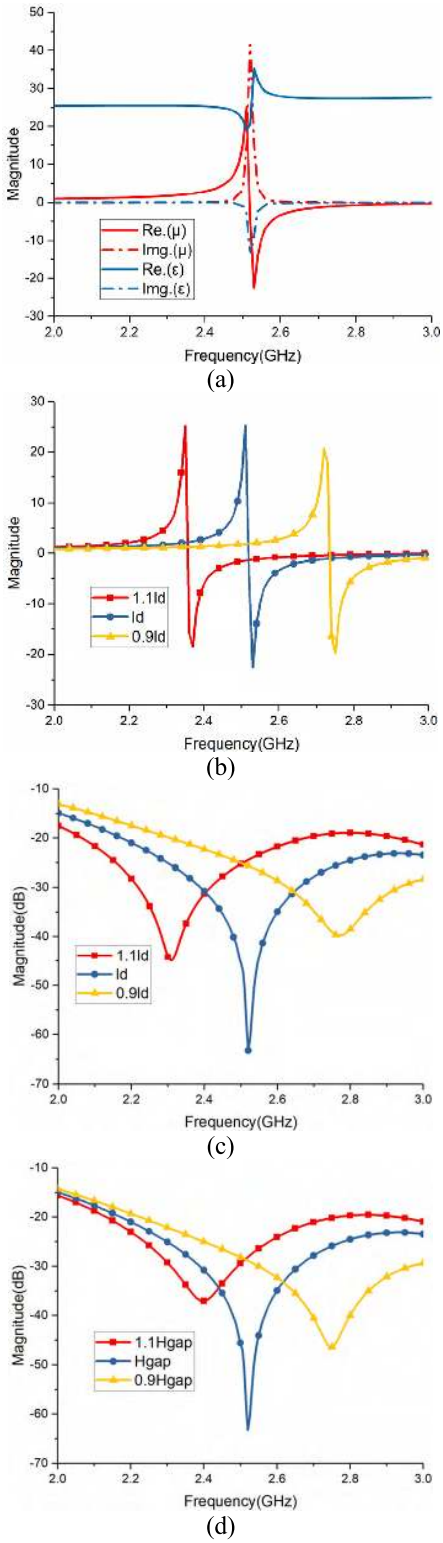

FIGURE 4. (a) Extracted permittivity and permeability of the metasurface using double layer cut wires as unit cell. (b) Extracted permeabilities with respect to different cut wire lengths. Decoupling frequency bands with respect to (c) different cut wire lengths and (d) different heights of the metasurface.

B. META-SURFACE DESIGN

In order to improve the isolation of the initial coupled antennas, a metasurface composed of pairs of cut wires is

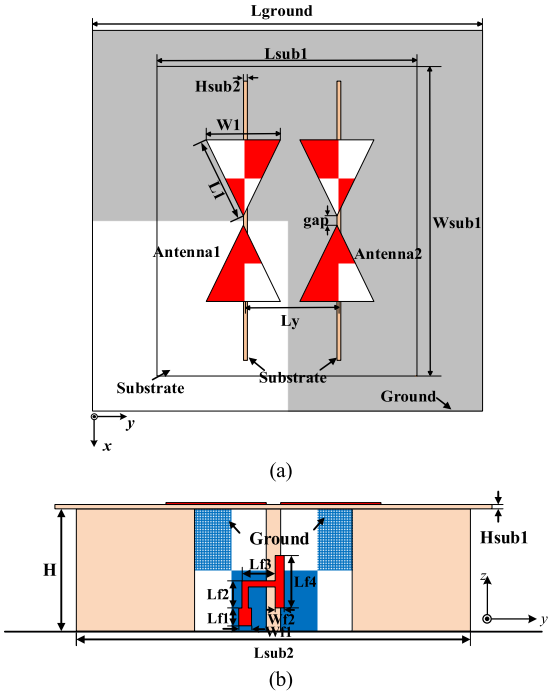

FIGURE 5. (a) Top view and; (b) Side view of the initial two bowtie antennas with T-probe feed structure.

TABLE 1. Detail dimensions of the coupled antennas (unit: mm).

Variable	Value	Variable	Value	Variable	Value
Lsub1	100	L1	32	Lf1	3.5
Wsub1	122	W1	15	Lf2	4.3
Lsub2	110	gap	3	Lf3	9.8
Hsub	1	Lground	150	Lf4	12.7
H	34	Wf1	2.1	Wf2	1.7

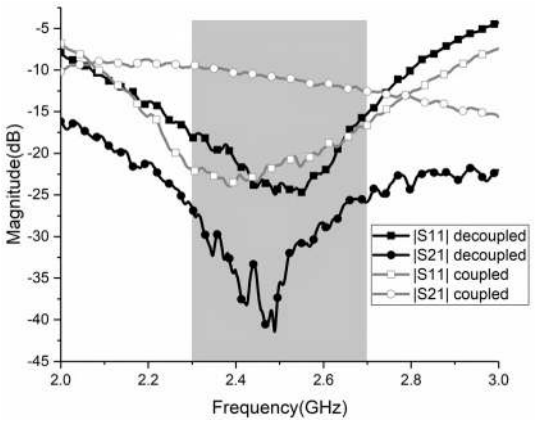

FIGURE 6. Measured S-parameters of the coupled and decoupled antennas.

introduced as the superstrate above the two antennas. The cut wire pairs are printed on a F4B substrate having height 0.8 mm with the relative dielectric constant of 2.65 and the loss tangent of 0.002 as shown in Fig. 7. The height of the

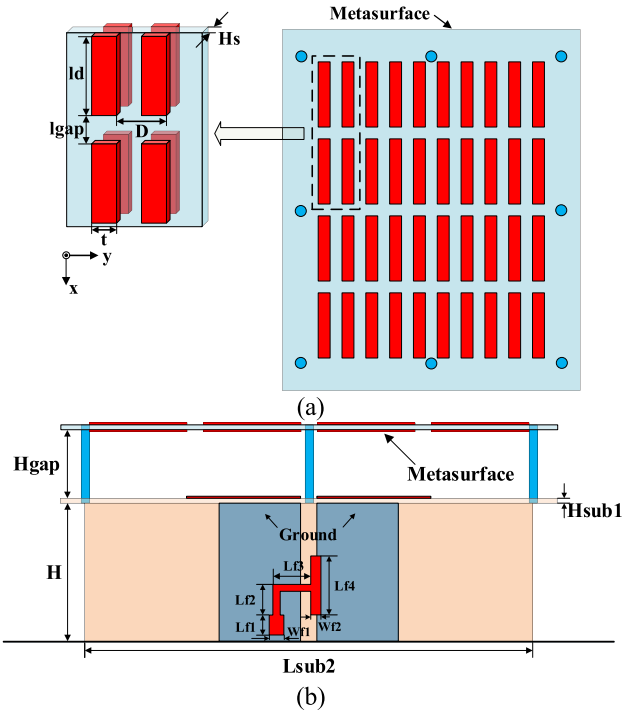

FIGURE 7. (a) Top view of the proposed metasurface using double layer cut wires; (b) Side view of the two bowtie antennas with T-probe feed structure with the proposed metasurface superstrate.

TABLE 2. Detail dimensions of the proposed antenna (unit: mm).

Variable	Value	Variable	Value
Lsub1	100	L1	36
Wsub1	122	W1	15
Lsub2	110	gap	3
Hsub	1	Lground	150
H	36	Wf1	2.2
Lf1	3.5	Hgap	15
Lf2	4.5	ld	25.1
Lf3	9.7	lgap	5.8
Lf4	12.7	t	3.4
Wf2	1.8	D	8.1

metasurface is designed to be Hgap = 15mm ($0.125\lambda_0$ at 2.5GHz). Since the metasurface superstrate will definitely affect the initial matching condition, the antenna geometry as well as the feed structure are then modified to meet the matching specification, which is conducted after the two antennas are successfully decoupled.

Other detail dimensions of the metasurface and the proposed antenna are shown in Table 2. The measured S-parameters are also superposed in Fig. 6. From Fig. 6, it is clear that the isolation between two antennas has been successfully improved to above 25dB within the band of 2300MHz to 2690MHz while the matching performance is well maintained below −15dB.

Then the decoupling performance is also parametrically analyzed. Antenna isolation performance with respect to

different cut wire lengths is studied. The results are already shown in Fig. 4 (b) and (c). As can be seen from the plots, the parameter *ld*, the length of the cut wire pair is essential to the overall decoupling performance, which is consistent with equation (3) and our previous discussion. Therefore, the decoupling band can be easily manipulated by changing the length of the cut wires as shown in Fig. 4 (c).

In the actual antenna system, the parameter *Hgap*, the height of the metasurface is also a design parameter. As shown in Fig.4 (d), improper height will affect the isolation of the antennas with the metasurface as well.

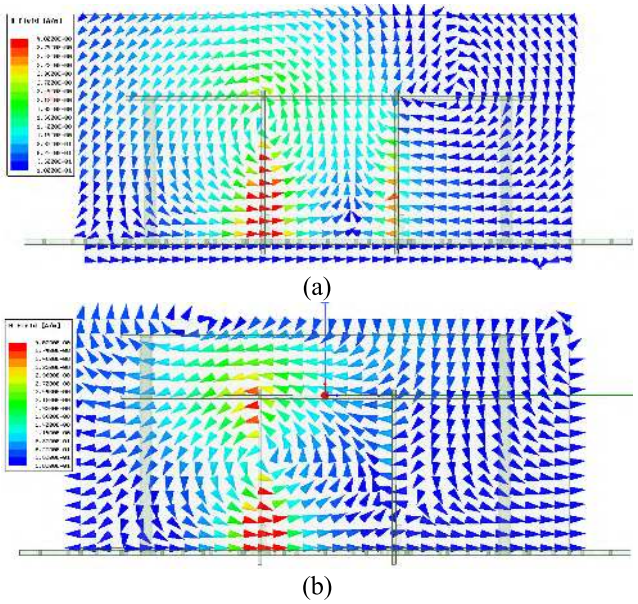

FIGURE 8. Simulated vector magnetic field distribution when antenna 1 is excited for coupled antennas (a) without the metasurface; and (b) with the metasurface.

To reveal the working mechanism, simulated vector magnetic field and magnitude of electric field are both plotted on a *yoz* cutting plane in the center of the feeding gap of the bowtie antennas. The field distributions are given in Fig. 8 and Fig. 9 respectively. The H-field components become horizontally arranged after inserting the metasurface superstrate, with E-field distributed along the x-direction, it is obvious the wave will mostly propagate along positive z-direction rather than coupled to the other antenna, which is consistent with the illustration in Fig. 1. From Fig. 9, it can be seen that the metasurface is able to create a forbidden region for one antenna while only the other antenna is excited.

C. PERFORMANCE EVALUATION

To evaluate the decoupling performance, the simulated antenna isolation with respect to different center to center antenna spacing is plotted in Fig. 10, as the spacing increases, the isolation is reduced from 15dB to around 25dB within the band of interest. In Fig. 10, the measured isolation with the metasurface is also plotted, which is even better than

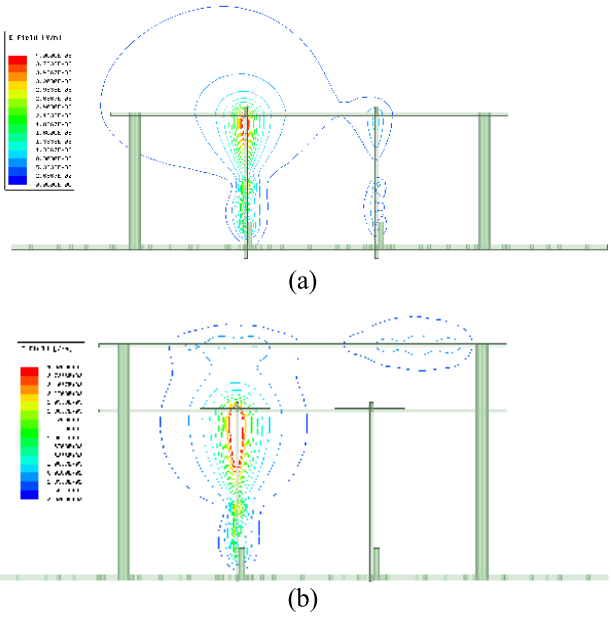

FIGURE 9. Simulated magnitude of electric field distribution when antenna 1 is excited for coupled antennas (a) without the metasurface; and (b) with the metasurface.

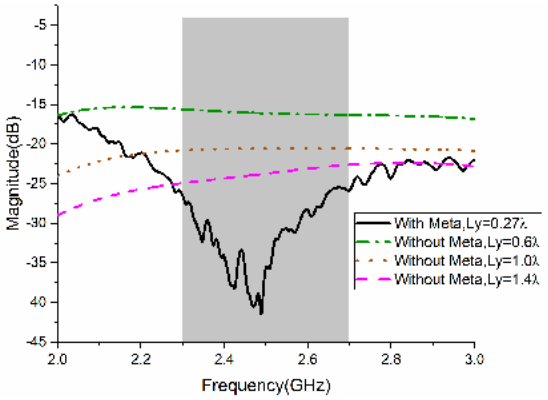

FIGURE 10. Simulated isolation of two bowtie antennas with different center to center spacing compared with the antennas with the metasurface superstrate.

the isolation of two antennas with the spacing of 1.4λ and without any metasurface.

The radiation patterns of the arrays with and without metasurface are measured in SATIMO 24 probe near field scanner as shown in Fig. 11. In the measurement process, both antennas are independently excited with the other antenna terminated with matched load. To validate our measurement results, they are compared with simulated ones in the first place as shown in Fig. 12. A good agreement between simulated and measured results has been observed.

Then, the measured radiation patterns at 2.3GHz, 2.5GHz and 2.7GHz are all plotted in Fig. 13∼15. It can be observed that the radiation patterns in different interested frequencies remain stable. And the peak gain of the antennas with the metasurface is improved by at most 2.5dB compared

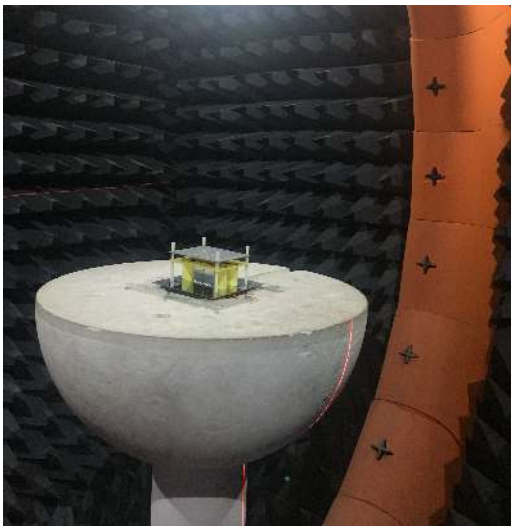

FIGURE 11. The configuration of radiation pattern measurement.

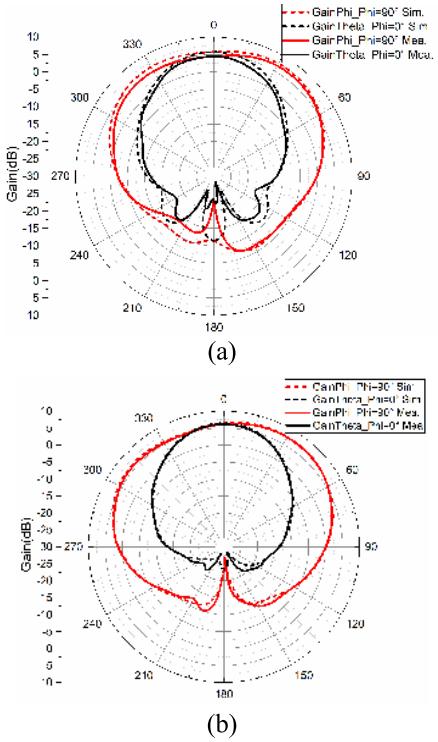

FIGURE 12. Simulated and Measured radiation patterns of the two antennas at 2.5 GHz (a) without and; (b) with metasurface.

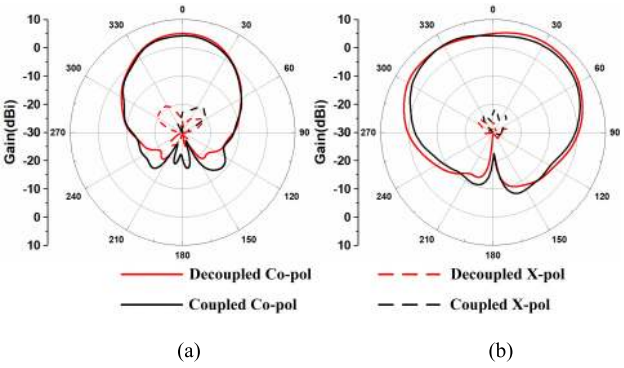

FIGURE 13. Measured radiation patterns for the arrays at 2.3 GHz without and with metasurface while port 1 is excited: (a) Phi = 0° cutting plane and; (b) Phi = 90° cutting plane.

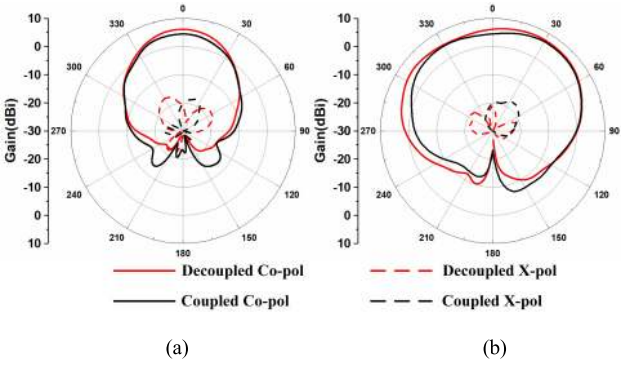

FIGURE 14. Measured radiation patterns for the arrays at 2.5 GHz without and with metasurface while port 1 is excited: (a) Phi = 0° cutting plane and; (b) Phi = 90° cutting plane.

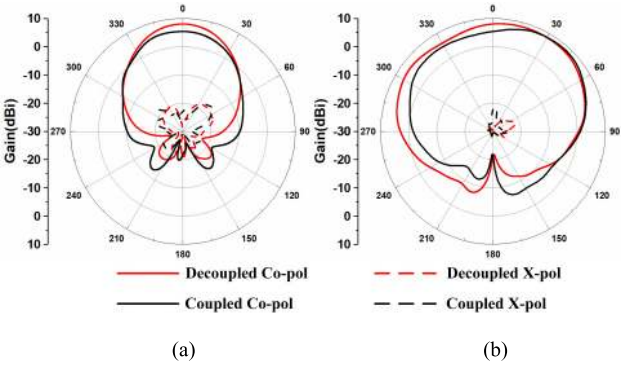

FIGURE 15. Measured radiation patterns for the arrays at 2.7 GHz without and with metasurface while port 1 is excited: (a) Phi = 0° cutting plane and; (b) Phi = 90° cutting plane.

to the antennas without the metasurface. Another important observation from Fig. 13∼15 is that the cross polarization discriminations of initial antenna are not deteriorated after adding the metasurface superstrate. Since the two antennas are in a nearly symmetrical form, the radiation patterns should also be in an almost symmetrical manner while the two ports are independently excited respectively, which is displayed in Fig. 16.

In order to illustrate the changes in the performances of the antenna with and without metasurface more intuitively, the specific values of the measured antenna E-plane radiation patterns of the different interested frequencies are given in Table 3. From Table 3, it can be seen that the peak gain of the antenna with metasurface is improved in the premise of a stable cross polarization discrimination. Moreover, the front-back-ratio (FBR) is also enhanced after adding the metasurface.

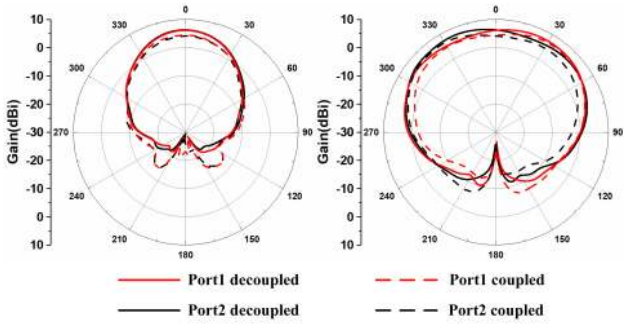

FIGURE 16. Measured radiation patterns for the antennas while the two antenna ports are independently excited at 2.5 GHz without and with metasurface, (a) Phi = 0° cutting plane and; (b) Phi = 90° cutting plane.

TABLE 3. Specific values of the antenna E-plane radiation patterns without meta-surface (E-plane).

Frequency	2.3GHz	2.5GHz	2.7GHz
Peak Gain	4.2dBi	4.5dBi	5.4
3dB Beamwidth	60°	59°	58°
XPD	>20dB	>19dB	>22dB
FBR	24dB	27.6dB	27.2dB
With Meta-surface (E-plane)			
Frequency	2.3GHz	2.5GHz	2.7GHz
Peak Gain	5.0dBi	6.1dBi	8.0
3dB Beamwidth	58°	52°	50°
XPD	>22dB	>20dB	>25dB
FBR	35.6dB	38.5dB	29dB

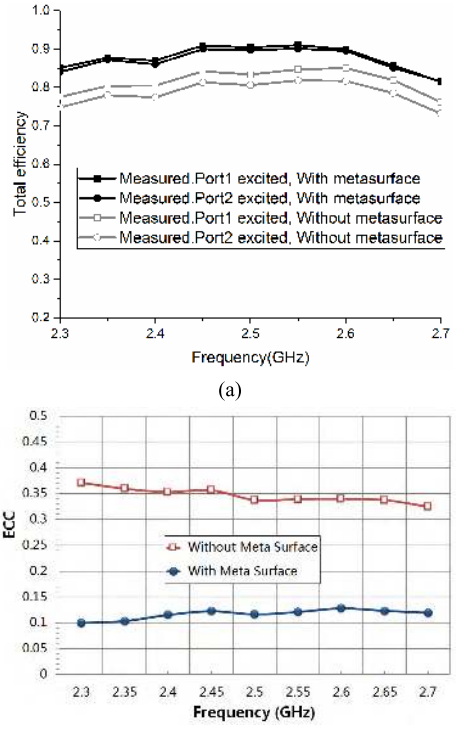

FIGURE 17. Measured (a) total efficiencies; and (b) ECCs for the two antennas without and with metasurface.

As shown in Fig. 17 (a), the total efficiency for the antennas with metasurface is 10% higher as compared to the ones without metasurface. This is because the isolation between the two antennas is increased and the mutual coupling is reduced, allowing more energy to be radiated along the normal radiation direction into the free space. The envelop correlation coefficient (ECC) is an important indicator in MIMO antenna systems. which can be written mathematically as:

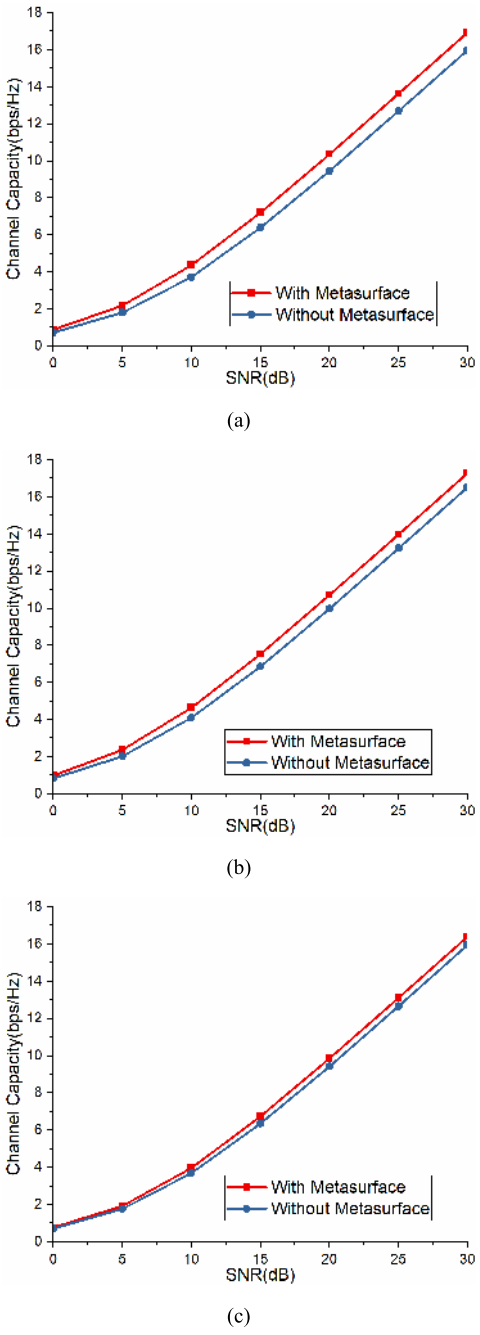

FIGURE 18. Calculated channel capacity with and without metasurface at (a) 2.3 GHz, (b) 2.5GHz and (c) 2.7GHz.

$$\rho_e = \frac{\left| \iint_{4\pi} \left[\vec{E}_1(\theta,\phi) \cdot \vec{E}_2(\theta,\phi) \right] d\Omega \right|^2}{\iint_{4\pi} \left| \vec{E}_1(\theta,\phi) \right|^2 d\Omega \iint_{4\pi} \left| \vec{E}_2(\theta,\phi) \right|^2 d\Omega} \tag{4}$$

with

$$\vec{E}_1(\theta,\phi)\cdot\vec{E}_2(\theta,\phi) = E_{\theta 1}(\theta,\phi)E^*_{\theta 2}(\theta,\phi) + E_{\phi 1}(\theta,\phi)E^*_{\phi 2}(\theta,\phi) \quad (5)$$

where $\boldsymbol{E}_1(\theta, \varphi)$ is the electric field of Antenna 1 while Antenna 2 is terminated with a matched load. Similarly, $\boldsymbol{E}_2(\theta, \varphi)$ is the electric field of Antenna 2 with Antenna 1 terminated.

The calculated ECCs without and with metasurface are shown in Fig. 17 (b). It can be seen that the ECC is reduced from 0.35 to 0.13 after the metasurface is added.

To obtain channel performance of the antennas, we have calculated the channel capacity according to [47]. Fig. 18 shows the calculated channel capacity with and without metasurface at 2.3GHz, 2.5GHz and 2.7GHz, respectively. As can be seen from the figures, the calculated channel capacity is effectively improved over the entire frequency band after adding the meta-surface superstrate.

IV. CONCLUSION

This paper introduces a brand new antenna decoupling method using the metasurface superstrate. Instead of using its previous SRR version in [43], double layer cut wires are used as unit cell of the metasurface since they are both compact in size and incident angle invariant. The proposed method is able to decouple two bowtie antennas with only 0.27-wavelength spacing in about 16% fractional bandwidth with 25dB isolation and about 0.12 ECC across the whole band. The method has the potential to be extend to linear arrays with more elements, rectangular arrays with both E and H coupling to be dealt with and eventually dual-polarized arrays. The related researches are still undergoing and their results will be reported in the future.

REFERENCES

[1] E. G. Larsson, O. Edfors, F. Tufvesson, and T. L. Marzetta, "Massive MIMO for next generation wireless systems," *IEEE Commun. Mag.*, vol. 52, no. 2, pp. 186–195, Feb. 2014.

[2] M. A. Jensen and J. W. Wallace, "A review of antennas and propagation for MIMO wireless communications," *IEEE Trans. Antennas Propag.*, vol. 52, no. 11, pp. 2810–2824, Nov. 2004.

[3] X. Chen, S. Zhang, and Q. Li, "A review of mutual coupling in MIMO systems," *IEEE Access*, vol. 6, pp. 24706–24719, Apr. 2018.

[4] J. B. Andersen and H. H. Rasmussen, "Decoupling and descattering networks for antennas," *IEEE Trans. Antennas Propag.*, vol. AP-24, no. 6, pp. 841–846, Nov. 1976.

[5] S. Chang, Y.-S. Wang, and S.-J. Chung, "A decoupling technique for increasing the port isolation between two strongly coupled antennas," *IEEE Trans. Antennas Propag.*, vol. 56, no. 12, pp. 3650–3658, Dec. 2008.

[6] L. Zhao, L. K. Yeung, and K.-L. Wu, "A coupled resonator decoupling network for two-element compact antenna arrays in mobile terminals," *IEEE Trans. Antennas Propag.*, vol. 62, no. 5, pp. 2767–2776, May 2014.

[7] L. Zhao and K.-L. Wu, "A dual-band coupled resonator decoupling network for two coupled antennas," *IEEE Trans. Antennas Propag.*, vol. 63, no. 7, pp. 2843–2850, Jul. 2015.

[8] L. Zhao, F. Liu, X. Shen, G. Jing, Y.-M. Cai, and Y. Li, "A high-pass antenna interference cancellation chip for mutual coupling reduction of antennas in contiguous frequency bands," *IEEE Access*, vol. 6, pp. 38097–38105, Jul. 2018.

[9] Y. Yu and H. T. Hui, "Design of a mutual coupling compensation network for a small receiving monopole array," *IEEE Trans. Microw. Theory Techn.*, vol. 59, no. 9, pp. 2241–2245, Sep. 2011.

[10] L. K. Yeung and Y. E. Wang, "Mode-based beamforming arrays for miniaturized platforms," *IEEE Trans. Microw. Theory Techn.*, vol. 57, no. 1, pp. 45–52, Jan. 2009.

[11] Y.-F. Cheng and K.-M. Cheng, "A novel dual-band decoupling and matching technique for asymmetric antenna arrays," *IEEE Trans. Microw. Theory Techn.*, vol. 66, no. 5, pp. 2080–2089, May 2018.

[12] L. Zhao, K.-W. Qian, and K.-L. Wu, "A cascaded coupled resonator decoupling network for mitigating interference between two radios in adjacent frequency bands," *IEEE Trans. Microw. Theory Techn.*, vol. 62, no. 11, pp. 2680–2688, Nov. 2014.

[13] L. Li, F. Huo, Z. Jia, and W. Han, "Dual zeroth-order resonance antennas with low mutual coupling for MIMO communications," *IEEE Antennas Wireless Propag. Lett.*, vol. 12, pp. 1692–1695, Dec. 2013.

[14] S. M. Amjadi and K. Sarabandi, "Mutual coupling mitigation in broadband multiple-antenna communication systems using feedforward technique," *IEEE Trans. Antennas Propag.*, vol. 64, no. 5, pp. 1642–1652, May 2016.

[15] S. Zhang and G. F. Pedersen, "Mutual coupling reduction for UWB MIMO antennas with a wideband neutralization line," *IEEE Antennas Wireless Propag. Lett.*, vol. 15, pp. 166–169, 2016.

[16] Z. Li, Z. Du, M. Takahashi, K. Saito, and K. Ito, "Reducing mutual coupling of MIMO antennas with parasitic elements for mobile terminals," *IEEE Trans. Antennas Propag.*, vol. 60, no. 2, pp. 473–481, Feb. 2012.

[17] L. Zhao and K.-l. Wu, "A decoupling technique for four-element symmetric arrays with reactively loaded dummy elements," *IEEE Trans. Antennas Propag.*, vol. 62, no. 8, pp. 4416–4421, Aug. 2014.

[18] G. Zhai, Z. N. Chen, and X. Qing, "Mutual coupling reduction of a closely spaced four-element MIMO antenna system using discrete mushrooms," *IEEE Trans. Microw. Theory Techn.*, vol. 64, no. 10, pp. 3060–3067, Oct. 2016.

[19] K.-L. Wu, C. Wei, X. Mei, and Z.-Y. Zhang, "Array-antenna decoupling surface," *IEEE Trans. Antennas Propag.*, vol. 65, no. 12, pp. 6728–6738, Dec. 2017.

[20] S. Zhang, B. K. Lau, Y. Tan, Z. Ying, and S. He, "Mutual coupling reduction of two PIFAs with a T-shape slot impedance transformer for MIMO mobile terminals," *IEEE Trans. Antennas Propag.*, vol. 60, no. 3, pp. 1521–1531, Mar. 2012.

[21] J. OuYang, F. Yang, and Z. M. Wang, "Reducing mutual coupling of closely spaced microstrip MIMO antennas for WLAN application," *IEEE Antennas Wireless Propag. Lett.*, vol. 10, pp. 310–313, Apr. 2011.

[22] Q. Li, A. P. Feresidis, M. Mavridou, and P. S. Hall, "Miniaturized double-layer EBG structures for broadband mutual coupling reduction between UWB monopoles," *IEEE Trans. Antennas Propag.*, vol. 63, no. 3, pp. 1168–1171, Mar. 2015.

[23] C.-Y. Chiu, C.-H. Cheng, R. D. Murch, and C. R. Rowell, "Reduction of mutual coupling between closely-packed antenna elements," *IEEE Trans. Antennas Propag.*, vol. 55, no. 6, pp. 1732–1738, Jun. 2007.

[24] K. Wei, J.-Y. Li, L. Wang, Z. Xing, and R. Xu, "Mutual coupling reduction by novel fractal defected ground structure bandgap filter," *IEEE Trans. Antennas Propag.*, vol. 64, no. 10, pp. 4328–4335, Oct. 2016.

[25] C.-Y. Chiu, F. Xu, S. Shen, and R. D. Murch, "Mutual coupling reduction of rotationally symmetric multiport antennas," *IEEE Trans. Antennas Propag.*, vol. 66, no. 10, pp. 5013–5021, Oct. 2018.

[26] C. F. Ding, X. Y. Zhang, C.-D. Xue, and C.-D. Sim, "Novel pattern-diversity-based decoupling method and its application to multielement MIMO antenna," *IEEE Trans. Antennas Propag.*, vol. 66, no. 10, pp. 4976–4985, Oct. 2018.

[27] H. Li, B. K. Lau, Z. Ying, and S. He, "Decoupling of multiple antennas in terminals with chassis excitation using polarization diversity, angle diversity and current control," *IEEE Trans. Antennas Propag.*, vol. 60, no. 12, pp. 5947–5957, Dec. 2012.

[28] P. Liang and Q. Wu, "Characteristic mode analysis of antenna mutual coupling in the near field," *IEEE Trans. Antennas Propag.*, vol. 66, no. 7, pp. 3757–3762, Jul. 2018.

[29] X. Zhao, S. P. Yeo, and L. C. Ong, "Decoupling of inverted-F antennas with high-order modes of ground plane for 5G mobile MIMO platform," *IEEE Trans. Antennas Propag.*, vol. 66, no. 9, pp. 4485–4495, Sep. 2018.

[30] F. Yang and Y. R. Samii, "Microstrip antennas integrated with electromagnetic band-gap (EBG) structures: A low mutual coupling design for array applications," *IEEE Trans. Antennas Propag.*, vol. 51, no. 10, pp. 2936–2946, Oct. 2003.

[31] E. Rajo-Iglesias, Ó. Quevedo-Teruel, and L. Inclan-Sanchez, "Mutual coupling reduction in patch antenna arrays by using a planar EBG structure and a multilayer dielectric substrate," *IEEE Trans. Antennas Propag.*, vol. 56, no. 6, pp. 1648–1655, Jun. 2008.

[32] S. D. Assimonis, T. V. Yioultsis, and C. S. Antonopoulos, "Design and optimization of uniplanar EBG structures for low profile antenna applications and mutual coupling reduction," *IEEE Trans. Antennas Propag.*, vol. 60, no. 10, pp. 4944–4949, Oct. 2012.
[33] M. J. Al-Hasan, T. A. Denidni, and A. R. Sebak, "Millimeter-wave compact EBG structure for mutual coupling reduction applications," *IEEE Trans. Antennas Propag.*, vol. 63, no. 2, pp. 823–828, Feb. 2015.
[34] J.-Y. Lee, S.-H. Kim, and J.-H. Jang, "Reduction of mutual coupling in planar multiple antenna by using 1-D EBG and SRR structures," *IEEE Trans. Antennas Propag.*, vol. 63, no. 9, pp. 4194–4198, Sep. 2015.
[35] Z. Qamar, U. Naeem, S. A. Khan, M. Chongcheawchamnan, and M. F. Shafique, "Mutual coupling reduction for high-performance densely packed patch antenna arrays on finite substrate," *IEEE Trans. Antennas Propag.*, vol. 64, no. 5, pp. 1653–1660, May 2016.
[36] P. V. Prasannakumar, M. A. Elmansouri, and D. S. Filipovic, "Wideband decoupling techniques for dual-polarized bi-static simultaneous transmit and receive antenna subsystem," *IEEE Trans. Antennas Propag.*, vol. 65, no. 10, pp. 4991–5001, Oct. 2017.
[37] B. C. Pan and T. J. Cui, "Broadband decoupling network for dual-band microstrip patch antennas," *IEEE Trans. Antennas Propag.*, vol. 65, no. 10, pp. 5595–5598, Oct. 2017.
[38] D. V. B. M. Trindade, C. Mũller, M. C. F. De Castro, and F. C. C. De Castro, "Metamaterials applied to ESPAR antenna for mutual coupling reduction," *IEEE Antennas Wireless Propag. Lett.*, vol. 14, pp. 430–433, Oct. 2014.
[39] M.-C. Tang *et al.*, "Mutual coupling reduction using meta-structures for wideband, dual-polarized, and high-density patch arrays," *IEEE Trans. Antennas Propag.*, vol. 65, no. 8, pp. 3986–3998, Aug. 2017.
[40] M. Farahani, J. Pourahmadazar, M. Akbari, M. Nedil, A. R. Sebak, and T. A. Denidni, "Mutual coupling reduction in millimeter-wave MIMO antenna array using a metamaterial polarization-rotator wall," *IEEE Antennas Wireless Propag. Lett.*, vol. 16, pp. 2324–2327, Jun. 2017.
[41] H. M. Bernety and A. B. Yakovlev, "Reduction of mutual coupling between neighboring strip dipole antennas using confocal elliptical metasurface cloaks," *IEEE Trans. Antennas Propag.*, vol. 63, no. 4, pp. 1554–1563, Apr. 2015.
[42] M. Akbari, H. Abo Ghalyon, M. Farahani, A.-R. Sebak, and T. A. Denidni, "Spatially decoupling of CP antennas based on FSS for 30-GHz MIMO systems," *IEEE Access*, vol. 5, pp. 6527–6537, Apr. 2017.
[43] Z. Wang, L. Zhao Cai, S. Zheng, and Y. Yin, "A meta-surface antenna array decoupling (MAAD) method for mutual coupling reduction in a MIMO antenna system," *Sci. Rep.*, vol. 8, Feb. 2018, Art. no. 3152.
[44] J. Zhou, L. Zhang, G. Tuttle, T. Koschny, and C. M. Soukoulis, "Negative index materials using simple short wire pairs," *Phys. Rev. B, Condens. Matter*, vol. 73, no. 4, p. 041101, Jan. 2006.
[45] Z. Szabo, G.-H. Park, R. Hedge, and E.-P. Li, "A unique extraction of metamaterial parameters based on Kramers Kronig relationship," *IEEE Trans. Microw. Theory Techn.*, vol. 58, no. 10, pp. 2646–2653, Oct. 2010.
[46] Y. Gou, S. Yang, J. Li, and Z. Nie, "A compact dual-polarized printed dipole antenna with high isolation for wideband base station applications," *IEEE Trans. Antennas Propag.*, vol. 62, no. 8, pp. 4392–4395, Aug. 2014.
[47] J. X. Yun and R. G. Vaughan, "Multiple element antenna efficiency and its impact on diversity and capacity," *IEEE Trans. Antennas Propag.*, vol. 60, no. 2, pp. 529–539, Feb. 2012.

FENG LIU received the B.S. degree in electronic information engineering from Xidian University, Xi'an, China, in 2016, where he is currently pursuing the Ph.D. degree in electromagnetic wave and microwave technology.

JIAYIN GUO received the B.S. degree in electronic information engineering from Xidian University, Xi'an, China, in 2016, where she is currently pursuing the Ph.D. degree in electromagnetic wave and microwave technology.

LUYU ZHAO was born in Xi'an, China, in 1984. He received the B.Eng. degree from Xidian University, Xi'an, in 2007, and the Ph. D. degree from The Chinese University of Hong Kong, Hong Kong, in 2014. He has been an Associate Professor with the National Key Laboratory of Antennas and Microwave Technology, Xidian University, since 2016.

From 2007 to 2009, he was with the Key Laboratory of Antennas and Microwave Technology, Xidian University, as a Research Assistant, where he was involved in the software and hardware implementation of RF identification technologies. From 2014 to 2015, he was a Post-Doctoral Fellow with The Chinese University of Hong Kong. From 2015 to2016, he was with Wyzdom Wireless Co. Ltd., where he was a Co-Founder and CTO. His current research interests include design and application of multiple antenna systems for next generation mobile communication systems, innovative passive RF and microwave components and systems, millimeter-wave and terahertz antenna array, and meta-material based or inspired antenna arrays.

Dr. Zhao was a recipient of the Best Student Paper Award of the 2013 IEEE 14th HK AP/MTT Postgraduate Conference and the Honorable Mention Award of the 2017 Asia-Pacific Conference on Antenna and Propagation.

XIUMEI SHEN received the B.S. degree in electronic information engineering and the master's degree in electromagnetic wave and microwave technology from Xidian University, Xi'an, China, in 2007 and 2010, respectively, where she is currently pursuing the Ph.D. degree in electromagnetic wave and microwave technology.

YINGZENG YIN received the B.S., M.S., and Ph.D. degrees in electromagnetic wave and microwave technology from Xidian University, Xi'an, China, in 1987, 1990, and 2002, respectively. From 1990 to 1992, he was a Research Assistant and an Instructor with the Institute of Antennas and Electromagnetic Scattering, Xidian University, where he was an Associate Professor with the Department of Electromagnetic Engineering, from 1992 to 1996, a Professor, since 2004. His current research interests include the design of microstrip antennas, feeds for parabolic reflectors, artificial magnetic conductors, phased array antennas, and computer-aided design for antennas.